Rheology of dry, partially saturated and wet granular materials

Pakpour, M.

Publication date
2013

2.

Dissipation in wet and dry granular materials

Abstract: In this chapter we review viscoelastic properties of materials and explain different experimental methods of studying the linear and non-linear behaviour of matter under shear tests. Then we investigate the stress-strain behaviour of sand with and without small amounts of liquid under steady and oscillatory shear. Since dry sand has a lower shear modulus, one would expect it to deform more easily. Using a new technique to quasi-statically push the sand through a tube with an enforced parabolic (Poiseuille-like) profile, we minimize the effect of avalanches and shear localization. We observe that the resistance against deformation of the wet (partially saturated) sand is much smaller than that of the dry sand, and that the latter dissipates more energy under flow. This is also observed in large amplitude oscillatory shear measurements using a rotational rheometer, showing that the effect is robust and holds for different types of flow.

2.1 Linear viscoelastic behaviour

Viscoelasticity is a result of simultaneous viscous and elastic properties in a material. Understanding the rheological behaviour of complex suspensions is an essential step in understanding the technological significance of their viscoelastic properties [4, 42].

Development of the mathematical theory of linear viscoelasticity is based on a superposition principle. This implies that the response (e.g. strain) at any time is directly proportional to the value of the initiating signal (e.g. stress). In the linear theory of viscoelasticity, the differential equations are linear. Also, the coefficients of the time differentials are constant. These constants are material parameters, such as the viscosity coefficient and rigidity modulus, and they are not allowed to change with changes in variables such as strain or strain rate. Further, the time

derivatives are ordinary partial derivatives. This restriction has the consequence that linear theory is applicable only to small changes in the variables. We can now generate a general differential equation for linear viscoelasticity as follows:

$$(1 + \alpha_1 \frac{\partial}{\partial t} + \alpha^2 \frac{\partial^2}{\partial t^2} + ... + \alpha_n \frac{\partial^n}{\partial t^n})\sigma = (\beta_0 + \beta_1 \frac{\partial}{\partial t} + \beta_2 \frac{\partial^2}{\partial t^2} + ... + \beta_m \frac{\partial^m}{\partial t^m})\gamma \quad (2.1)$$

Some important special cases of Eq. 2.1 follow. For example if β_0 is the only non-zero parameter, $\sigma = \beta_0\gamma$, which is the equation of Hookean elasticity and β_0 is called the rigidity modulus, G. For the only non-zero parameter β_1, we have the Newtonian viscous flow and this parameter shows the coefficient of viscosity, η.

If just both α_1 and β_1 are non-zero, the Eq. 2.1 leads to the "Kelvin model" which is one of the simplest models of viscoelasticity:

$$\sigma = G\gamma + \eta\dot{\gamma}. \quad (2.2)$$

Another simple model is the "Maxwell model". The differential equation for the model is: $\sigma + \alpha_1\dot{\sigma} = \eta\dot{\gamma}$, where $\alpha_1 = \tau_M = \eta/G$ called the relaxation time.

The next level of complexity in the linear viscoelastic behaviour is to make other parameters of Eq. 2.1 non-zero. These kind of equations can be derived mathematically for different suspensions with viscoelastic behaviour. In addition, many other ideas have been employed to develop elementary models for viscoelastic behaviour. The response of the material to a linear or constant input parameter (e.g. stress or strain) is obtained by solving Eq. 2.1 and its variants.

2.1.1 Oscillatory shear tests

A key to measuring the linear and non-linear viscoelastic behaviour of the materials is the determination of their response to small amplitude oscillatory shears (SAOS), which weakly perturb the equilibrium structure, and large amplitude oscillatory shears (LAOS) [43, 44].

Dynamic oscillatory shear tests are common in rheology and have been used to investigate a wide range of soft matter and complex fluids including polymer melts, biological macromolecules, polymers, surfactants, suspensions, emulsions and beyond. Although small amplitude oscillatory shear is a popular deformation mode in probing the linear viscoelastic behaviour of materials, the useful properties of soft materials are often related to their responses to high strains [1, 45, 46].

Large amplitude oscillatory shear (LAOS) is a class of flow that is commonly used to characterize nonlinear viscoelastic material behaviour. The first studies of LAOS refer to early publications in the $1960s$ to $1970s$. The methods for analysing LAOS include Lissajous curves (Philippoff 1966; Tee and Dealy 1975), Fourier transform rheology (e.g., Wilhelm 2002), stress decomposition (Cho *et al.* 2005; Ewoldt *et al.* 2008; Yu *et al.* 2009), and computation of viscoelastic moduli (Hyun et al. 2002; Ewoldt et al. 2008). In this thesis, the physical meaning of the LAOS

measurements is highlighted by considering graphically the raw test data in the form of Lissajous curves, which are plots of stress $\sigma(t)$ vs. strain $\gamma(t)$ [44].

Both the elastic and viscous characteristics of a material can be examined simultaneously by imposing an oscillatory shear strain. An oscillatory strain at fixed frequency is applied to the sample and consequently subjects the sample to a corresponding oscillatory strain rate:

$$\gamma(t) = \gamma_0 \sin(\omega t), \qquad \dot{\gamma}(t) = \gamma_0 \omega \cos(\omega t), \tag{2.3}$$

where ω is the frequency of rotation and γ_0 is the strain amplitude which is small enough for the linearity constraint to be satisfied. The strain amplitudes used in linear oscillatory shear tests are very small, often of the order of $\gamma_0 \approx 10^{-2}$ and for some emulsions or suspensions the linear regime is limited to even smaller than this value. Then the stress response to this input deformation $\sigma(t; \omega, \gamma_0)$ is recorded and analysed. So the LAOS measurements are defined by two input parameters, frequency and amplitude $\{\omega, \gamma_0\}$ and the response of the material in terms of stress can be written as:

$$\sigma(t) = \gamma_0[G' \sin(\omega t) + G'' \cos(\omega t)]. \tag{2.4}$$

When γ_0 is constant, the linear viscoelastic response is observed. For ideal solids that follow Hooke's law, the shear strain is proportional to the shear stress and the functions are in phase (Fig. 2.1 (a)). For the ideal fluids that follow Newton's law of viscosity, the shear rate is proportional to the shear stress with the phases shifted by 90^o (Fig. 2.1 (b)). For the viscoelastic materials the shear stress function can be separated into an elastic stress in phase with the shear strain, and a viscous stress in phase with the shear rate (Fig. 2.1 (c)).

The storage modulus is the ratio of the elastic stress to shear strain while the loss modulus is the ratio of the viscous stress to shear strain. At low strain amplitudes when the response is linear, the material is commonly characterized by the viscoelastic moduli G' and G'' as determined from the components of the stress in phase with γ and $\dot{\gamma}$, respectively. The constant storage modulus G' and the loss modulus G'' are defined in the linear viscoelastic regime, and their values at high strain amplitude need care in the measurements to find the $G'(\gamma_0)$ and $G''(\gamma_0)$.

The dependence of storage and loss moduli on strain amplitude is interpreted as a non-linear viscoelastic response. The material's resistance to deformation is the complex shear modulus G^* consisting of an elastic or storage modulus (G') and a viscous or loss modulus (G''):

$$G^* = G' + iG''. \tag{2.5}$$

The oscillatory test responses can be described as Lissajous curves with stress versus strain that provide a meaningful way to visualize and understand viscoelastic behaviour in general. A linear elastic material response, $\sigma = G\gamma$, appears as a straight line on the Lissajous curve of $\sigma(t)$ versus $\gamma(t)$ and in the linear viscoelastic regime, the Lissajous figures are elliptical when the stress response is a sinusoidal function with a phase difference $0 < \delta < \pi/2$ compared with the strain (Fig. 2.1).

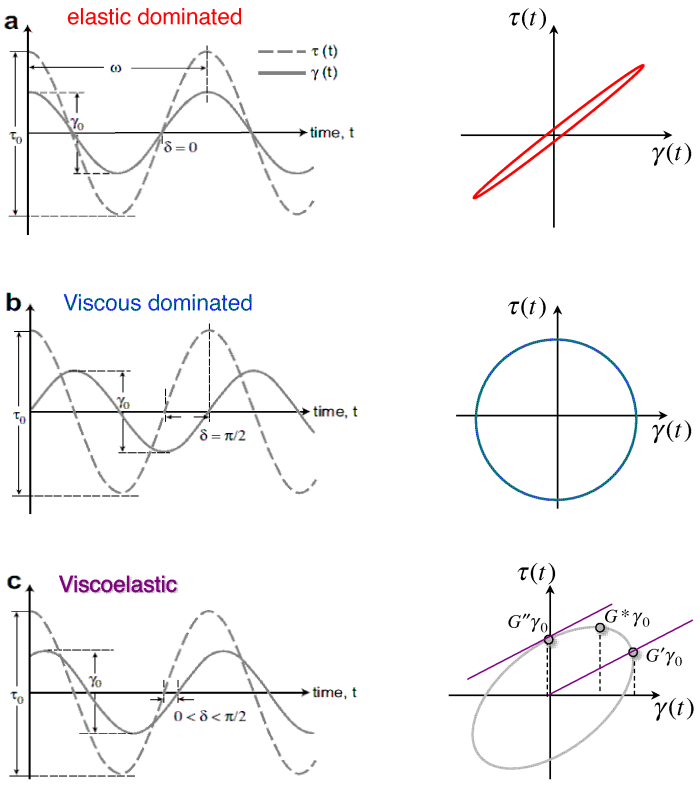

Figure 2.1: Plot of the imposed sinusoidal stress function (dashed) and recorded shear strain (solid) in dynamic oscillatory tests for an (a) ideal elastic, (b) viscous and (c) viscoelastic material. $\sigma(t)$ is the dynamic shear stress function, σ_0 is the amplitude of the stress function, $\gamma(t)$ is the dynamic shear strain function, γ_0 is the amplitude of the strain function, ω is the frequency of the imposed oscillation, and δ is the phase shift angle between shear stress and shear strain [47].

The strain amplitude γ_0 can be increased systematically to enter the non-linear viscoelastic regime. A non-linear viscoelastic response will change the elliptical shape of a Lissajous curve with the deviation from linear viscoelastic behaviour. When the strain amplitude γ_0 becomes large, for an oscillatory strain input, $\gamma(t) = \gamma_0 \sin(\omega t)$, the viscoelastic stress response can be written as a Fourier series of odd harmonics:

$$\sigma(t;\omega,\gamma_0) = \gamma_0 \sum_{n:odd} G'_n(\omega,\delta_0)\sin(n\omega t) + G''_n(\omega,\delta_0)\cos(n\omega t). \tag{2.6}$$

For sufficiently small strain amplitude γ_0, a linear material response is observed such that only the fundamental harmonic appears, $n = 1$ with a temporal phase shift δ_1 given by $\tan\delta_1 = G''_1/G'_1$ [48,49]. For larger deformation amplitudes, higher

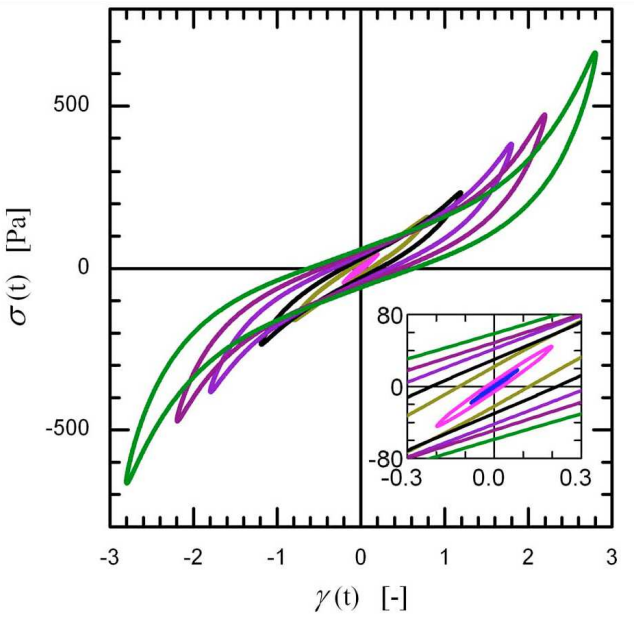

Figure 2.2: Oscillatory strain sweeps of pedal mucus gel from *Limax maximus* [50] at a frequency $\omega = 3$ rad.s^{-1} which shows the plotting of the raw data of $\sigma(t)$ versus $\gamma(t)$ reveals nonlinear characteristics of this gel. Inset: the linear behaviour in low strain [48].

harmonics appear, and the response is nonlinear.

Figure 2.2 shows the raw data and the corresponding non-linear behaviour of $\sigma(t)$ and $\gamma(t)$. In this work, a series of oscillatory tests at a fixed frequency of $\omega = 3$ rad.s^{-1} are imposed and the corresponding nonlinear behavior of the physically cross-linked mucus gel is shown [47]. The inset shows a linear viscoelastic response appearing as an ellipse for small γ_0, which contains the major and minor axes of the ellipse and the nonlinear viscoelastic response loses the elliptical shape [44, 45, 48, 49].

2.2 Flow of wet and dry granular materials

In Section 1.4.2 we discussed the different regimes of wetting in granular matter and showed that the small amount of liquid added to a dry granular material which forms "bridges" at the contact points between the grains, changes the mechanical properties of these matters. In Chapter 3 we investigate dry granular media and also the impact of the amount of fluid in the granular media and its effect on the strength of a wet granular material. For dry sand, a major step in describing the rheological properties was the introduction of the Coulomb friction approach

[51–53]. This relates the shear stress to the confinement pressure via a friction coefficient [54].

Wet (partially saturated) granular materials have been studied mostly in the geophysics literature since soils are a typical example of such a system. Here, the characterization of flow properties is very different; these materials are reported to exhibit a mixed behaviour of elasticity, viscosity, and plasticity. The system starts to flow when the externally imposed stress exceeds the inter-aggregate contact forces [55]. The mechanical properties at lower water content are determined by the liquid bridges between grains, and those at higher water content are determined by the flow of the liquid through the soil pores [56].

In this chapter we compare the properties in incipient flows of wet and dry granular materials near the jamming transition. Partially saturated granular matter has a much higher yield-stress (allowing the construction of a sand castle) and should therefore have a much higher apparent viscosity for slow flows [57, 58]. It means that above a critical yield-stress, the mechanical response changes from a solid-like to a dissipative flow. The microscopic mechanism for this behaviour refering to the reorganization of individual particles that resists the motion and the microstructure present in the fluid that resists large rearrangements is responsible for the yield-stress. For this reason, it is commonly believed that wet sand should show a larger resistance to flow, i.e., more viscous, than dry sand [18, 26, 59].

We will show, however, that in two very different set-ups, the energy dissipation, is larger than that of wet sand. We show that this is due to the fact that the adhesion between the grains decreases the confining pressure and hence decreases the flow resistance.

2.3 Experimental techniques

2.3.1 Shear cell

This experiment were carried out using sand composed of glass spheres of diameter $d = 140 - 150$ μm with and without additional deionized water. The water content ω is defined as the ratio between the liquid volume and the volume occupied by the grains. The experiments were carried out with the shear cell described in references [19, 60]. The experimental works relevant to the shear cell have been carried out in collaboration with the Saarland University. The use of this device makes it possible to shear the granular materials homogeneously over the sample volume.

The granular material is put into an acrylic cylindrical cell (Fig. 2.3(a)). A cylindrical cell made of acrylic glass and with a diameter equal to its length $L = D = 24$ mm, was filled with the sample (brown). The "flat sides" of the cell each consist of a thin latex membrane with a thickness of 300 μm. Adjacent to each membrane was a cylindrical chamber filled with water connected to a syringe. So the sample is separated from the confining water (in the chamber) by the flexible

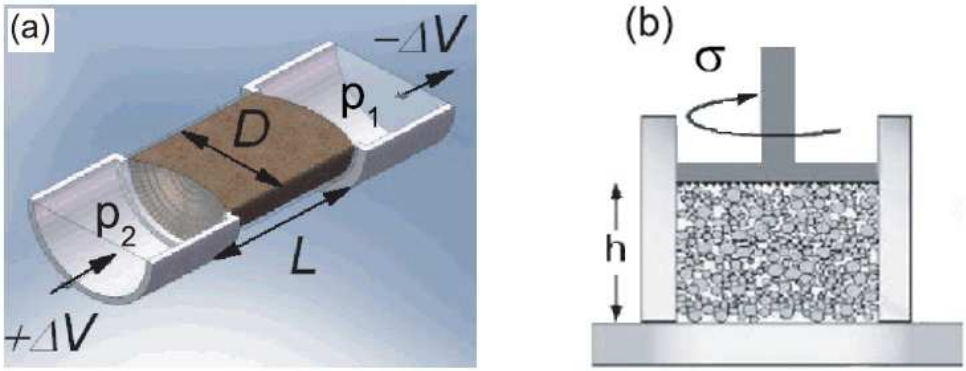

Figure 2.3: (a) Tube experiments measurement cell containing granular matter (brown); a volume change ΔV provokes a difference between p_1 and p_2, the pressures in the adjacent chambers; D and L, are the cell diameter and length, respectively. (b) Cup-plate rotational rheometric set-up.

membrane. Also the membrane transfers the presure to the confined sand in the cell.

Dry sand gently was poured into the cell and the density corresponding to that of random dense packing $\phi = 0.63$, was achieved by tapping the sand in the cell. The cell was also filled with wet sand with $0.01 \leq \omega \leq 0.3$ and $\phi = 0.63$. It was possible to inject water into and extract it from the chamber through tubes via a syringe. The syringe pistons were connected to spindles that could be moved with a step motor.

When the two pistons were moved at equal speed and in opposite directions, the sample between the membranes was deformed at constant volume and well defined speed. The tension of the membranes had approximately parabolic deformation, and and imposes a Poiseuille-like profile within the sample. In this way, avalanching was kept to a minimum, and a rather homogeneous shear deformation of the sample is achieved. Piezoresistive sensors measure the pressure (with respect to atmospheric pressure) in both chambers. A fixed quantity of water was then injected into or extracted from the adjacent chambers, and the differential pressure $p_1 - p_2$ was measured. A family of differential pressure characteristics for increasing shear volumes is shown in Fig. 2.4.

It is worth mentioning that for a given shear amplitude, the hysteresis loop is stable during as many cycles. A few tests were carried out which were one week in duration and found that the opening of the loop for different shear amplitudes remains constant (we made sure that all our data were taken in such a steady-state situation). Also the shear rates $\dot{\gamma}$ were tested between 0.0002 and 0.1 s^{-1} without observing differences in the hysteresis loop. The measured quantities for

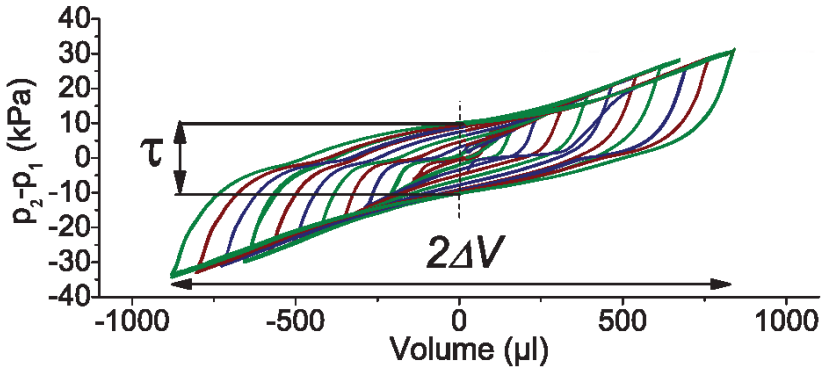

Figure 2.4: Differential pressure curves with increasing shear amplitudes for wet sand. The measured parameters for each curve are σ and ΔV.

each differential pressure curve are the opening of the loop at zero shear σ and the volume ΔV. The imposed profile permited us to estimate the equivalent for the wall shear strain for the cylindrical cell as $\gamma_{max} = 32\Delta V/\pi D^3$ [61].

Strain γ is the input parameter which we apply on the system and then we obtain the response of the material to this excitation, which is shear stress. In the oscillatory form of deformation (or strain-controlled deformation) we have an reciprocating motion which in these tests the strain changes by time according to the strain amplitude during a cycle. So we can define the maximum value of γ during a loop of a reciprocating motion.

2.3.2 Oscillatory shear tests

For a better understanding of the results and to check their robustness, I performed a similar experiment in a completely different geometry. This approach emphasizes the visual representation of the LAOS stress response and enables us to explore how the material properties characterizing the dessipated energy depend on size of the grains and liquid volume fraction. Also oscillatory measurements are suitable tests to characterize the macroscopic response related to the microstructure of a material.

For this, I used a standard rheometer with a geometry that allows a test under confinement. I used cup-plate geometry (Fig. 2.3 (b)) and studied polystyrene spheres (Dynoseeds) with diameters $140, 250$ and 500 μm, with and without additional silicon oil. I used silicon oil rather than water as polystyrene beads are not wettable by water with volume fractions $\omega = 0.01$ and 0.04. The beads were poured into the cup of the rheometer (50 mm diameter and 5mm bed depth) with a global packing fraction $\phi \simeq 0.63$ (Fig. 2.3 (b)).

The rheometric equivalent of the differential pressure displacement curves are the so-called Lissajous curves, where one plots the stress as a function of the deforma-

tion for a single oscillation cycle of the plate. In this set-up, we investigated the energy dissipated in a Lissajous cycle which represents the resistance of the dry or wet granular media against the flow. Typical Lissajous characteristics are shown in Figs. 2.7 (b)-(d) for the dry and wet polystyrene beads [62].

This is observed that the results from shear cell and oscillatory test for different types of flow, are in good agreement.

2.4 Results

2.4.1 Energy for flowing granular materials

The surprising conclusion from the shear cell experiments is that the wet sand flows more easily than the dry. This is evident from the pressure-displacement curves shown Fig. 2.7 (a). The area enclosed by the pressure/strain curve is directly proportional to the work done, i.e., the energy dissipated during the cycle [44]. Therefore for the same overall deformation, the dissipated energy is much smaller for the wet than for the dry sand. Figure 2.5 shows σ versus γ_{max}, these measurements were taken for samples prepared with different packing fractions and liquid contents ω. Compaction of a granular assembly is the reduction of its free volume when it is submitted to mechanical vibrations.

Recent studies have shown that the liquid bridges which determine the mechanical properties of granular systems, (dependent on the liquid content) exhibits a maximum in the range $0.01 \leq w < 0.03$. It was confirmed also by using X-ray tomography that the onset for the coalescence of liquid bridges occurs around a critical water content of $w \approx 0.025$ [19].

Figure 2.5 shows that for small deformations ($\gamma_{max} < 0.1$), we found that dry sand does not resist any stress to within the accuracy of the experiment. On the other hand, the wet sand behaves like a yield-stress fluid due to the liquid bridge network. For the almost completely dry and almost completely wet mixtures the yield-stress is quite low and the grains reach something resembling close packing when poured into the rheometer geometry, but for the intermediate liquid volume fractions the yield-stress is quite high and the material does not compact under its own weight giving much lower grain filling fractions [26, 63].

Accordingly, the inset in Fig. 2.5 shows the range $\gamma_{max} < 0.1$, from which we get a mean value $\langle\sigma\rangle = (1.2 \pm 0.4)$ kPa for the wet sand and $\langle\sigma\rangle = (1.2 \pm 0.4)$ kPa for the dry sand. For the wet sand this value keeps constant in the range of existence of the liquid bridge network $0.01 \leq \omega \leq 0.03$; in good agreement with Ref. [64]. In this paper Scheel *et al.* investigate the mechanical properties of the pile which are largely independent of the amount of liquid over a wide range [65–68]. They resolved this puzzle with the help of X-ray microtomography and showed that the remarkable insensitivity of the mechanical properties to the liquid content is due to the particular organization of the liquid in the pile into open structures.

Figure 2.6 (a) shows data for three characteristic mechanical parameters of a wet pile of the glass beads. The tensile strength, and the critical acceleration at which

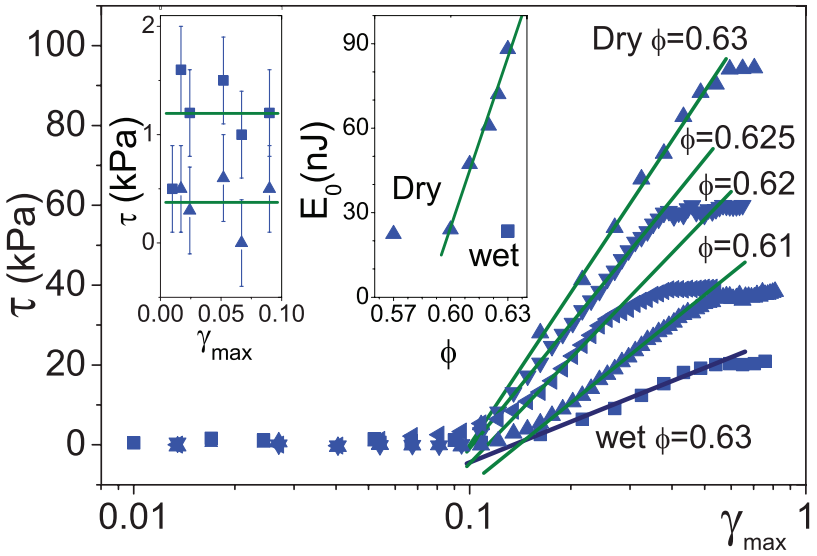

Figure 2.5: Studies with the tube experiment, σ vs. γ_{max} behaviour and corresponding fit for the dissipative flow range for dry sand with different packing fractions ϕ and wet sand ($0.01 \leq \omega \leq 0.03, \phi = 0.63$). The left inset shows the corresponding range $\gamma_{max} < 0.1$. The right inset shows the characteristic energy E_0 versus the packing fraction ϕ (triangles) compared with the wet sand (squares).

fluidization sets in are plotted as a function of liquid content, ω, in the range $0 < \omega \leq 0.15$. These results show that there is a sharp rise at very small ω, where the transition from the dry state to the wetted state (capillary bridges) takes place. Figure 2.6 (b) shows the liquid distribution and formation of the capillary bridges between the grains. Actually the number of capillary bridges, the total number of liquid clusters (defined as connected regions of liquid wetting more than two beads) and the liquid volume of the biggest cluster are shown as functions of the liquid content. Clearly, substantial changes in the morphology of the liquid structures take place in the studied range. As ω is increased, the liquid structures merge into larger clusters [64]. In Fig. 2.5 the onset of dissipative flow occurs for deformations larger than about $\gamma_{onset} \sim 0.1$ in all cases; this suggests that it is the size of the grains rather than the presence or absence of the network that sets this strain scale. Further, σ grows more strongly for the dry than for the wet sand (Fig. 2.5), this means that one needs less energy to push the wet sand through the tube. To quantify this, we note that beyond the yield point in Fig. 2.5, the data show an exponential dependence of the deformation on the stress:

$$\frac{\gamma_{max}}{\gamma_{onset}} = \exp(\frac{\sigma}{\sigma_0}). \tag{2.7}$$

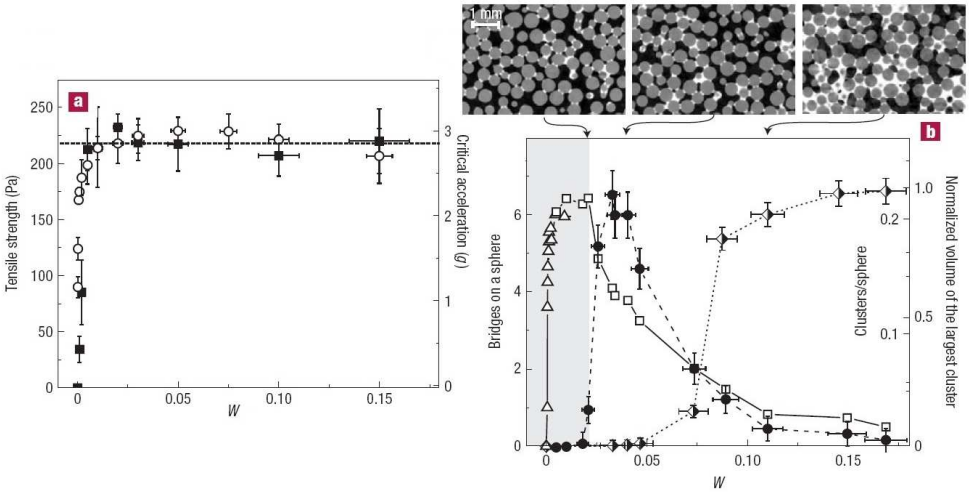

Figure 2.6: Stiffness of a wet granular pile in comparison with the reorganization of liquid structures. (a) Mechanical properties: tensile strength (filled squares), critical acceleration for fluidization (open circles). The dashed horizontal line is a guide to the eye. (b) Images: sections through 3D tomograms of the analyzed samples at $\omega = 0.02, 0.04$ and 0.11, from left to right. Main panel: frequencies of liquid objects as extracted from X-ray tomography data. Left axis (open symbols): average number of capillary bridges on a sphere (triangles: by fluorescence microscopy and squares by X-ray tomography). Right axis: average number of clusters per sphere (filled symbols), and normalized volume of the largest cluster (half-filled symbols) [64].

A fit with Eq. 2.7, applied, for example, for dry and wet sand with $\phi = 0.63$, yields a constant $\sigma = 55$ and 14.7 kPa and onset values $\gamma_{onset} = 0.1$ and 0.14, respectively; with ν the volume of a grain, we define $E_0 = \sigma\nu$ and $E_0 = \sigma_0\nu$, so it is possible to rewrite Eq. 2.7 as:

$$\frac{\gamma_{max}}{\gamma_{onset}} = \exp(\frac{E}{E_0}), \tag{2.8}$$

where E_0 is an intensive property of the granular assembly, which in a mean-field picture includes all the interactions and possible configurations of the grains [69]. From the fits we then find $E_0 = 88$ and 23 nJ for the dry and wet granulate with $\phi = 0.63$, respectively. A mean-field meaning, all such interactions between regions, are subsumed into an effective "noise temperature" $E_0 = k_B\Theta$ [69–72]. This is based on the intuition that every yield event elsewhere in the material causes a kick locally via the associated stress redistribution, and that many such kicks add up to an effectively thermal noise. This is assumed to create a new local equilibrium configuration with correspondingly new yield energy. We expect these activated yield processes to arise primarily by coupling to structural rearrangements elsewhere in the system. In a mean-field spirit, all such interactions between regions

are subsumed into an effective noise temperature. The noise temperature, proposed phenomenologically to control the dynamics of a set of degrees of freedom. This parameter can be interpreted as a genuine non-equilibrium thermodynamic temperature, governing the degrees of freedom whose dynamics causes the system to move among its various inherent structures or energy minima [69, 71, 73].

It is difficult to estimate the value of Θ for dry sand since the energy loss is sensitive to, for example, microscopic roughness and topology. For increasing packing fractione, we measure ϕ a range of Θ until around 6 PK (peta Kelvin) as shown in the inset of Fig. 2.5, which is in agreement with previous measurements [70–72].

For the wet sand, Θ can be related directly to the liquid bridges. By considering the coordination number $n = 6$, the characteristic energy per bridge is $E_0/n = (4 \pm 2)$ nJ, which is in agreement with an estimate for the energy loss during bridge formation and rupture $\Delta E_{cap} < \pi\gamma_\omega d^2/2 = 2.4$ nJ [60, 63].

2.4.2 Energy dissipated in wet and dry granular matter

As I explened in the prior sections of this chapter, the non-linear behavior of materials in dynamic oscillations is characterized by a waveform of the output signal and this response of the material can be decomposed in a Fourier series. A Lissajous figure can be used to represent the variation of the stress versus strain in the oscillatory shear test. So the term Lissajous curve denotes the projection of the oscillatory response curves onto the stress $\sigma(t)$ versus strain $\gamma(t)$ plane.

The energy dissipated per unit volume in a single cycle of Lissajous curves, can be visualized by the area enclosed by the Lissajous curves [44]:

$$E_d = \oint \sigma d\gamma = \pi G'' \gamma_0^2, \tag{2.9}$$

For a linear viscoelastic material, G'' is independent of γ_0 and the dissipated energy is a quadratic function of the strain amplitude. In this case, the Lissajous figure is an ellipse. The non-linear viscoelastic behavior is also characterized by a departure from the elliptic form and the distortions increasing with strain amplitude. Contrary to a linear viscoelastic material, the energy versus strain amplitude is not a quadratic function. This curve for the perfect plastic materials is always a rectangle with a high dissipated energy in comparison with the purely elastic materials where E_d goes to zero [49].

Equivalently, in the shear cell measurements when pushing sand through the tube, one can calculate the energy dissipated in a single cycle as the area of the differential-pressure curve loop. Figure 2.7 (a) shows the energy dissipated in this experiment for dry and wet sand with liquid content $\omega = 0.03$.

Figures 2.7 (b)-(d) also present the stress vs. strain plots for dry and wet sand to investigate material hysteretic properties in viscoelastic solid mechanics. These measurements have been carried out for 500, 250 and 140 μm beads' diameter and different liquid content. Recall that the energy lost by viscous dissipation per unit

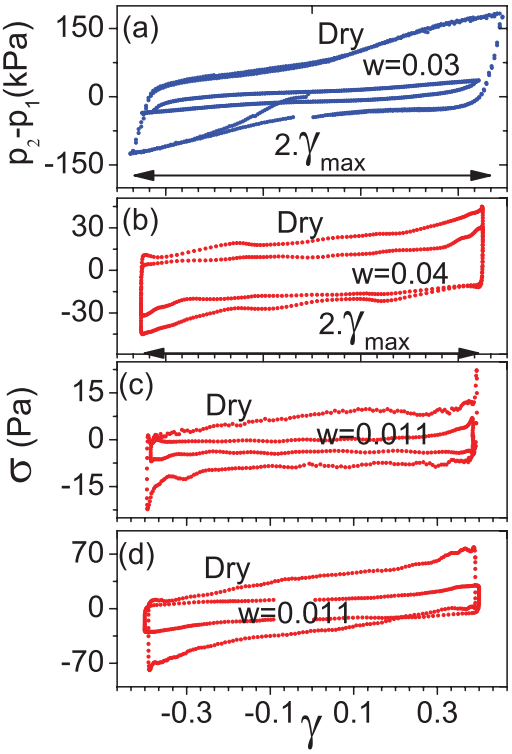

Figure 2.7: (a) Differential pressure curves for dry and wet sand measured with the set-up of Fig. 2.3 (a). In blocks (b)(d) Lissajous characteristics are shown for polystyrene beads with and without silicon oil under confinement measured with the standard rheometric set-up of Fig. 2.3 for bead diameters (b) 250, (c) 500, and (d) $140\mu m$. The liquid content ω indicates the wet loop. The strain amplitude γ_{max} is indicated in (a) and (b).

volume is given by Lissajous curves and this energy represents the amount of work required to deform a material. So we need more energy to push the dry sand for different type of materials and different conditions (i. e. liquid volume fraction in granular system).

By calculating the area enclosed by these Lissajous curves in Fig. 2.7, for two very different setups; shear cell and oscillatory test, we found that the dissipated energy for the wet sand is smaller than that of the dry and it means that wet sand feels less resistance aginst flow and consequently flows more easily. Physically, these hysteresis, or energy dissipation, is supposed due to the inter-granular friction during rearrangement of the grains, which is expected to depend on the strain amplitude and the confining pressure which influences the contact forces. The value of energy dissipated is strictly related to the nonlinear viscoelastic responses.

So we have examine the dissipated energy which is clearly related to the breakup

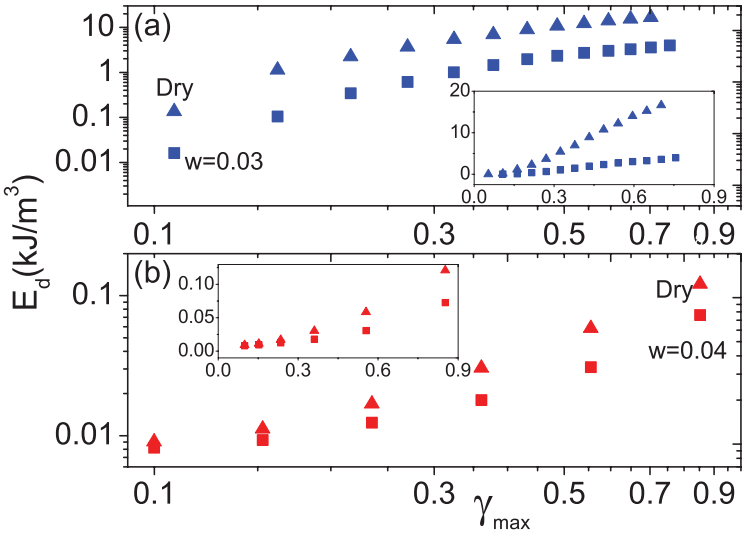

Figure 2.8: Dissipated energy per unit volume E_d versus strain amplitude γ_{max}: (a) for the range $\gamma_{max} > 0.1$, calculated from the area of the differential pressure curve loop; and (b) integrating E_d from Lissajous loops for polystyrene beads. In both figures, squares represent wet sand, and triangles dry sand. The insets show the same graphs in linear scale.

of the suspension structure. A comparison of two methods of experiments for dry and wet granular materials show that the resistance against flow for wet sand is much smaller than the dry sand and the cohesion arises from capillary force in the wet matter describe the behavior of these systems. The bridges between the grain create a network of grains that connected to each other by pendular bridges. These bridges leads to a force of attraction between the grains which is absent in dry granular materials and hold the granular system together. In this case this attractive force reduce the tendency of the system to dilate under flow and hence decreases the flow resistance of wet systems. So we note that the Lissajous curves would correspond to intersections and dissipative nature of the materials.

Surprisingly, we found that these results show that this conclusion is general for different materials and does not depend on the size of the beads and the liquid content of the wet sand.

Figure 2.8 shows the energy for deformations beyond the yield point for both experiments. The comparison of Figs. 2.8 (a) and (b) shows that the results are very similar qualitatively, but that a quantitative difference occurs in the measured dissipated energy. The differences in order of magnitude for E_d between the two experiments can be understood from both the differences between the two set-ups and those between the granular media.

2.5 Conclusion

The tube experiment is conceived in such a way that the deformation remains homogeneous throughout the sample. In the rheology set-up, on the other hand, for the larger deformations there is undoubtedly shear localization (banding) which in general happens because this is the easiest way for the system to deform, that is, the deformation that minimizes the dissipated energy. On the other hand, additional experiments for wet sand show that the opening of the loop σ varies inversely with the diameter of the beads and also depends on the surface tension. Thus, although the results from the two set-ups can only be compared in a qualitative manner, they do confirm the main result that the overall energy dissipation is smaller for wet than for dry sand.

The question remains then, why is this so? One possible explanation is the following: the sand should behave as a frictional granular system in the regime beyond yielding. When granular shear flows is prevented by confinement, shear is instead accompanied by normal forces. It is well known that for such systems, the shear stress under flow is directly proportional to the normal stress, i.e., the confining pressure. This is significant evidence supporting the significance of dilation and normal forces.

All the experiments have been carried out for the liquid volume fraction ranged between 0.01 and 0.04 which show the partially saturated regime of wetting. The liquid leads to the formation of capillary bridges at the contact points between the grains, and the surface energy (the curvature of the liquid interface) leads to capillary pressure causing a force of attraction between the grains which is absent in dry granular materials. The bridges which create a network of grains connected by pendular bridges are an adhesive force that hold the granular system together. In this case the suction force which is drawn back into the liquid under capillary action, should reduce the tendency of the system to dilate under flow, thus reducing the confining pressure.

In the tube experiment a measure of the confining pressure is the mean value of the sum of the pressures at maximum shear, $p = (|p_1 + p_2|_{-\gamma_{max}} + |p_1 + p_2|_{\gamma_{max}})/2$ is shown in Fig. 2.9 (a). The advantage of the rheometric set-up is that it provides us with a direct measurement of the confining pressure. In the rheology experiments, which were carried out with a fixed gap of the cup-plate geometry, the confining pressure is directly the normal stress measured by the rheometer during the deformation.

We have investigated the results by study the behavior of normal stress for dry and wet sand to see the frictional behavior in these systems. Figure 2.9 (b) shows the measured normal stress as a function of the deformation for dry and wet sand. It is evident that the normal stresses are much larger for dry sand: the dry sand is much more dilatant and this provides a direct explanation of why the wet sand flows more easily than the dry sand. The origin of dilatancy when granular matter are sheared is that each particle needs to find room in order for the system to flow, and the system thus expands. But in the wet granular matter the liquid bridges

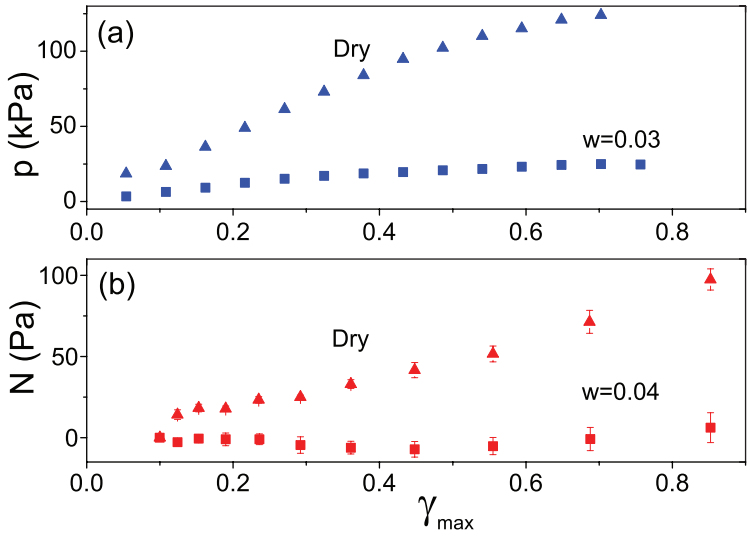

Figure 2.9: (a) Confinement pressure versus strain amplitude for the tube experiment. (b) Normal stress versus strain amplitude for the cup-plate rheometric set-up.

apply an adhesive force that hold the grains together and it redudce the normal force or dilatancy in these systems.

Both dry and wet systems are expected to have a friction coefficient that is constant and somewhat smaller than unity. Since for frictional systems, the friction coefficient is nothing more than the ratio of normal to shear forces, a smaller normal stress immediately implies a smaller shear stress, in line with the results presented above.

So, we have found that it is much easier to push wet sand than dry granular matter in a Poiseuille-like profile through a tube. Even if the capillary forces increase the yield-stress, the water promotes cluster formation and reduces effective intergrain friction, whereas for dry sand the yield-stress is zero and a pure frictional behaviour is observed.